High-Resolution Optical Vector Analysis Based on Symmetric Double-Sideband Modulation

Min Xue, *Member, IEEE*, Shifeng Liu, and Shilong Pan, *Senior Member, IEEE*

***Abstract*— An optical vector analyzer (OVA) based on symmetric optical double-sideband (ODSB) modulation using a phase modulator (PM) and an intensity modulator (IM) is proposed and demonstrated. In the symmetric-ODSB-based OVA, frequency response measurements are implemented by transmitting the phase-modulated and intensity-modulated ODSB signals through an optical device-under-test (DUT), respectively. Then, removing the responses of the two electro-optic modulators and processing the measured responses, accurate frequency responses of the DUT on both sides of the optical carrier are obtained. Comparing with the conventional OVA based on optical single-sideband (OSSB) modulation, the proposed ODSB-based OVA has the doubled measurement range and the simple wavelength-independent configuration. Moreover, the measurement system inherently has large dynamic range and high accuracy, which is difficult to achieve for the OSSB-based OVA due to the restriction of the limited sideband suppression ratio. An experiment for measuring the magnitude and the phase responses of a programmable optical filter is carried out. The responses in a range of 100 GHz are measured with a resolution of 10 MHz by using 50-GHz components.**

***Index Terms*— Microwave photonics, measurement techniques, electro-optic modulators, optical variables measurement**

I. Introduction

KNOWING the frequency responses including the magnitude and phase responses is of great importance for the fabrication and application of optical devices. To do so, methods based on a wavelength-swept laser source, such as the interferometry method [1]–[2] and the modulation phase-shift method [3], were proposed. Restricted by the low wavelength accuracy and poor wavelength stability of the wavelength-swept laser sources, the resolution is usually very low (in the order of hundreds of MHz), which is too coarse to achieve fine frequency responses of optical devices having the capability of manipulating the optical spectrum with MHz or even sub-MHz resolution. In order to achieve high-resolution measurement, optical vector analyzer (OVAs) based on optical single-sideband (OSSB) modulation were proposed and demonstrated [4]–[11]. Benefiting from the high-resolution microwave frequency sweeping and high-accuracy microwave phase-magnitude detection, tens-of-kHz resolution was experimentally demonstrated and sub-Hz resolution is theoretically achievable [4], [5]. The key challenge associated with the OSSB-based OVA, however, is to generate an OSSB signal with broad sweeping bandwidth and large sideband suppression ratio (SSR). The sweeping bandwidth determines the measurement range of the OVA and the SSR places a restriction on the measurement accuracy and the dynamic range [7]. In addition, it is incapable to measure bandpass responses due to the extremely exacerbated carrier-to-sideband ratio, since the optical carrier needs to be located outside of the bandpass responses.

To extend the measurement range and enhance the accuracy, OVAs based on asymmetric optical double-sideband (ODSB) modulation were developed [12]–[14], in which the wavelength of the optical carrier is shifted to avoid the frequency aliasing problem caused by the beat between the optical carrier and the sidebands. The measurement range is doubled and the measurement results are immune to the high-order-sideband induced errors. However, the complexity of the electrical-to-optical conversion and phase-magnitude detection is dramatically increased, as the up and down frequency conversions are required to extract the information from the beat signals.

In this letter, a symmetric-ODSB-based OVA employing a phase modulator (PM) and an intensity modulator (IM) is proposed and demonstrated, which features not only simple wavelength-independent electrical-to-optical conversion configuration but also broad measurement range which is twice the bandwidth of the components used in the OVA. Moreover, the proposed ODSB-based OVA inherently has large dynamic range and high accuracy. Similar to the OSSB-based and carrier-shifted-ODSB-based OVAs, the frequency sweeping and phase-magnitude extraction are accomplished in the electrical domain, so the feature of ultrahigh measurement resolution is preserved.

II. PRINCIPLE

Figure 1 shows the schematic diagram of the proposed ODSB-based OVA. A lightwave from a tunable laser source (TLS) is divided into two branches. One part is sent to a Mach-Zehnder modulator (MZM) and the other is

Manuscript received December 5, 2017; revised January 16, 2018; accepted January 25, 2018. Date of publication January 30, 2018; date of current version February 13, 2018. This work was supported in part by the National Natural Science Foundation of China under Grant 61705103, 61527820, and 61422108, and in part by the National Key Research and Development Program of China under Grant 2017YFF0106900. *(Corresponding author: Shilong Pan.)*

The authors are with the Key Laboratory of Radar Imaging and Microwave Photonics, Ministry of Education, Nanjing University of Aeronautics and Astronautics, Nanjing 210016, China (e-mail: pans@ieee.org).

Color versions of one or more of the figures in this letter are available online at http://ieeexplore.ieee.org.

Digital Object Identifier 10.1109/LPT.2018.2799565

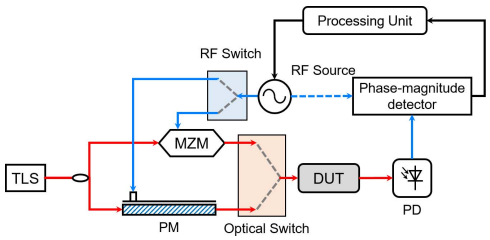

Fig. 1. Schematic diagram of the proposed ODSB-based OVA. TLS: tunable laser source; PM: phase modulator; MZM: Mach-Zehnder modulator; DUT: device-under-test; RF: radio frequency; PD: photodetector.

directed to a PM. Then, a two-step measurement is performed. In the first step, an intensity-modulated signal is generated by injecting the RF signal into the MZM. Then, after propagating through an optical device-under-test (DUT), the optical signal is received and converted into a photocurrent by a photodetector (PD). An electrical phase-magnitude detector extracts the magnitude and phase information of the AC term of the photocurrent. By sweeping the frequency of the RF source, a transmission function is measured, which is the vectorial sum of the frequency responses on the two sides of the optical carrier. In the second step, the RF signal is switched to the PM and a phase-modulated signal is produced. With a similar process, another transmission function, which is the vectorial subtraction of the frequency responses on the two sides of the optical carrier, is achieved. By removing the responses of the MZM and PM, accurate magnitude and phase responses of the DUT on both sides of the optical carrier can be achieved through simple post signal processing. Since there is no wavelength-dependent device (like optical filters) in the scheme, the proposed ODSB-based OVA can be seen as wavelength insensitive, which enables measurement at any center wavelength.

Mathematically, in a small signal modulation case, only the optical carrier and two first-order sidebands are considered, so the optical fields of the intensity-modulated signal from the MZM and the phase-modulated signal from the PM can be written as

$$\begin{aligned} E_{\mathrm{MZM}}(t) = {} & E_0 J_1(\beta_1) \exp\left[i(\omega_\mathrm{o}-\omega_\mathrm{e})t - i\frac{\pi}{4}\right] \\ & + E_0 J_0(\beta_1) \exp\left(i\omega_\mathrm{o} t + i\frac{\pi}{4}\right) \\ & - E_0 J_1(\beta_1) \exp\left[i(\omega_\mathrm{o}+\omega_\mathrm{e})t - i\frac{\pi}{4}\right] \quad (1) \\ E_{\mathrm{PM}}(t) = {} & -E_0 J_1(\beta_2) \exp\left[i(\omega_\mathrm{o}-\omega_\mathrm{e})t\right] \\ & + E_0 J_0(\beta_2) \exp(i\omega_\mathrm{o} t) \\ & + E_0 J_1(\beta_2) \exp\left[i(\omega_\mathrm{o}+\omega_\mathrm{e})t\right] \quad (2) \end{aligned}$$

where ω_o and ω_e are the angular frequencies of the optical carrier and the RF signal, respectively, E_0 is the amplitude of the optical carrier and $J_n(\bullet)$ is the nth-order Bessel function of the first kind, β_1 and β_2 are the modulation indices of the MZM and PM.

Transform the intensity-modulated and phase-modulated signals into the frequency domain, we have

$$\begin{aligned} E_{\mathrm{MZM}}(\omega) = {} & E_0 J_1(\beta_1) \exp\left(-i\frac{\pi}{4}\right) \delta[\omega-(\omega_\mathrm{o}-\omega_\mathrm{e})] \\ & + E_0 J_0(\beta_1) \exp\left(i\frac{\pi}{4}\right) \delta(\omega-\omega_\mathrm{o}) \\ & - E_0 J_1(\beta_1) \exp\left(-i\frac{\pi}{4}\right) \delta[\omega-(\omega_\mathrm{o}+\omega_\mathrm{e})] \quad (3) \\ E_{\mathrm{PM}}(\omega) = {} & -E_0 J_1(\beta_2) \delta[\omega-(\omega_\mathrm{o}-\omega_\mathrm{e})] \\ & + E_0 J_0(\beta_2) \delta(\omega-\omega_\mathrm{o}) \\ & + E_0 J_1(\beta_2) \delta[\omega-(\omega_\mathrm{o}+\omega_\mathrm{e})] \quad (4) \end{aligned}$$

When the intensity-modulated signal propagates through the DUT, the magnitude and phase of the three components are changed by the DUT, which can be expressed as

$$\begin{aligned} & E^{\mathrm{T}}_{\mathrm{MZM}}(\omega) \\ & = E_0 J_1(\beta_1) H(\omega_\mathrm{o}-\omega_\mathrm{e}) \exp\left(-i\frac{\pi}{4}\right) \delta[\omega-(\omega_\mathrm{o}-\omega_\mathrm{e})] \\ & \quad + E_0 J_0(\beta_1) H(\omega_\mathrm{o}) \exp\left(i\frac{\pi}{4}\right) \delta(\omega-\omega_\mathrm{o}) \\ & \quad - E_0 J_1(\beta_1) H(\omega_\mathrm{o}+\omega_\mathrm{e}) \exp\left(-i\frac{\pi}{4}\right) \delta[\omega-(\omega_\mathrm{o}+\omega_\mathrm{e})] \quad (5) \end{aligned}$$

where $H(\omega) = H_{\mathrm{DUT}}(\omega) \cdot H_{\mathrm{sys}}(\omega)$, $H_{\mathrm{DUT}}(\omega)$ is the transmission function of the DUT and $H_{\mathrm{sys}}(\omega)$ the transmission function of the optical path excluding the responses of the electro-optic modulators (EOMs).

After square-law detection in the PD, the ω_e component in the converted photocurrent is given by

$$\begin{aligned} & i_{\mathrm{MZM}}(\omega_\mathrm{e}) \\ & = \eta E_0^2 J_0(\beta_1) J_1(\beta_1) H(\omega_\mathrm{o}+\omega_\mathrm{e}) H^*(\omega_\mathrm{o}) \exp\left(i\frac{\pi}{2}\right) \\ & \quad + \eta E_0^2 J_0(\beta_1) J_1(\beta_1) H(\omega_\mathrm{o}) H^*(\omega_\mathrm{o}-\omega_\mathrm{e}) \exp\left(i\frac{\pi}{2}\right) \quad (6) \end{aligned}$$

where η is the responsivity of the PD. It should be noted the combined frequency responses of the MZM and PD can be measured via an electrical vector network analyzer (VNA), which is

$$H_{\mathrm{MZM}}(\omega_\mathrm{e}) = \eta E_0^2 J_0(\beta_1) J_1(\beta_1) \exp\left(i\frac{\pi}{2}\right) \quad (7)$$

Thus, (6) can be simplified as

$$\begin{aligned} i_{\mathrm{MZM}}(\omega_\mathrm{e}) = {} & H_{\mathrm{MZM}}(\omega_\mathrm{e}) H(\omega_\mathrm{o}+\omega_\mathrm{e}) H^*(\omega_\mathrm{o}) \\ & + H_{\mathrm{MZM}}(\omega_\mathrm{e}) H(\omega_\mathrm{o}) H^*(\omega_\mathrm{o}-\omega_\mathrm{e}) \quad (8) \end{aligned}$$

With the phase-modulated signal, a similar process is carried out, so another photocurrent is achieved with the electrical field can be written as

$$\begin{aligned} i_{\mathrm{PM}}(\omega_\mathrm{e}) = {} & H_{\mathrm{PM}}(\omega_\mathrm{e}) H(\omega_\mathrm{o}+\omega_\mathrm{e}) H^*(\omega_\mathrm{o}) \\ & - H_{\mathrm{PM}}(\omega_\mathrm{e}) H(\omega_\mathrm{o}) H^*(\omega_\mathrm{o}-\omega_\mathrm{e}) \quad (9) \end{aligned}$$

where $H_{\mathrm{PM}}(\omega_\mathrm{e})$ is the combined transmission function of the PM and PD, which is expressed as

$$H_{\mathrm{PM}}(\omega_\mathrm{e}) = \eta E_0^2 J_0(\beta_2) J_1(\beta_2) \quad (10)$$

and can be measured with the help of a calibrated phase modulation to intensity modulation (PM-IM) convertor.

According to (8) and (9), the transmission functions on both sides of the optical carrier can be achieved, which are

$$H(\omega_o+\omega_e)=\left[\frac{i_{MZM}(\omega_e)}{H_{MZM}(\omega_e)}+\frac{i_{PM}(\omega_e)}{H_{PM}(\omega_e)}\right]/2H^*(\omega_o) \quad (11)$$

$$H(\omega_o-\omega_e)=\left[\frac{i^*_{MZM}(\omega_e)}{H^*_{MZM}(\omega_e)}-\frac{i^*_{PM}(\omega_e)}{H^*_{PM}(\omega_e)}\right]/2H^*(\omega_o) \quad (12)$$

In order to remove the transmission function of the measurement system from the measured results, a calibration process is performed, in which the DUT is removed and the two test ports are directly connected, i.e. $H_{DUT}(\omega)$ =1. In this case, we have

$$H_{sys}(\omega_o+\omega_e)=\left[\frac{i_{sys,MZM}(\omega_e)}{H_{MZM}(\omega_e)}+\frac{i_{sys,PM}(\omega_e)}{H_{PM}(\omega_e)}\right]/2H^*_{sys}(\omega_o) \quad (13)$$

$$H_{sys}(\omega_o-\omega_e)=\left[\frac{i^*_{sys,MZM}(\omega_e)}{H^*_{MZM}(\omega_e)}-\frac{i^*_{sys,PM}(\omega_e)}{H^*_{PM}(\omega_e)}\right]/2H^*_{sys}(\omega_o) \quad (14)$$

From (11) to (14), we obtain the transmission functions of the DUT on both sides of the optical carrier,

$$\begin{aligned}H_{DUT}(\omega_o+\omega_e)&=\frac{H(\omega_o+\omega_e)}{H_{sys}(\omega_o+\omega_e)}\\&=\frac{\frac{i_{MZM}(\omega_e)}{H_{MZM}(\omega_e)}+\frac{i_{PM}(\omega_e)}{H_{PM}(\omega_e)}}{\left[\frac{i_{sys,MZM}(\omega_e)}{H_{MZM}(\omega_e)}+\frac{i_{sys,PM}(\omega_e)}{H_{PM}(\omega_e)}\right]H^*_{DUT}(\omega_o)}\end{aligned} \quad (15)$$

$$\begin{aligned}H_{DUT}(\omega_o-\omega_e)&=\frac{H(\omega_o-\omega_e)}{H_{sys}(\omega_o-\omega_e)}\\&=\frac{\frac{i^*_{MZM}(\omega_e)}{H^*_{MZM}(\omega_e)}-\frac{i^*_{PM}(\omega_e)}{H^*_{PM}(\omega_e)}}{\left[\frac{i^*_{sys,MZM}(\omega_e)}{H^*_{MZM}(\omega_e)}-\frac{i^*_{sys,PM}(\omega_e)}{H^*_{PM}(\omega_e)}\right]H^*_{DUT}(\omega_o)}\end{aligned} \quad (16)$$

where $H^*_{DUT}(\omega_o)$ is a constant since it is the frequency response of the DUT at a fixed wavelength.

III. Experiment Results

An experiment based on the setup shown in Fig. 1 is carried out. A lightwave with a power of 16 dBm is generated by a TLS (Agilent N7714A). A 40-Gbps single-drive MZM (Fujitsu) and a 40-Gbps PM (EOSPACE Inc), which have usable frequency responses to 50 GHz with no sharp response dips, are used to generate the intensity-modulated and phase-modulated signals. A 50-GHz PD (Finisar XPDV2120R) with a responsivity of 0.65 A/W is employed to convert the optical signal into a photocurrent. A programmable optical filter (Finisar WaveShaper 4000s) is served as the DUT. The frequency-swept RF signal and the electrical phase-magnitude detection are implemented by a 67-GHz VNA (R&S ZVA67). A modulator bias controller (MBC, YYLabs Inc.) is used to ensure that the MZM is biased at the quadrature point.

According to (15) and (16), to achieve the accurate responses of the DUT, the responses of the EOMs together with the PD and the optical paths, which are the inherent features of the system, should be pre-measured. Figure 2(a) and (b) are the magnitude and phase terms of the $H_{MZM}(\omega)$ (blue line) and $H_{PM}(\omega)$ (red line) from 10 MHz to 50 GHz. As can be seen, with the increase of the frequency, the efficiency of the electrical-optical and optical-electrical conversions decreases, which would lead to a reduced dynamic range at the high frequencies. Figure 2(c) and (d) show the magnitude and phase responses respectively measured by the phase-modulated and intensity-modulated signals without the DUT, which are exactly the responses of the optical paths, i.e. $i_{sys,MZM}(\omega_e)$ (blue line) and $i_{sys,PM}(\omega_e)$ (red line).

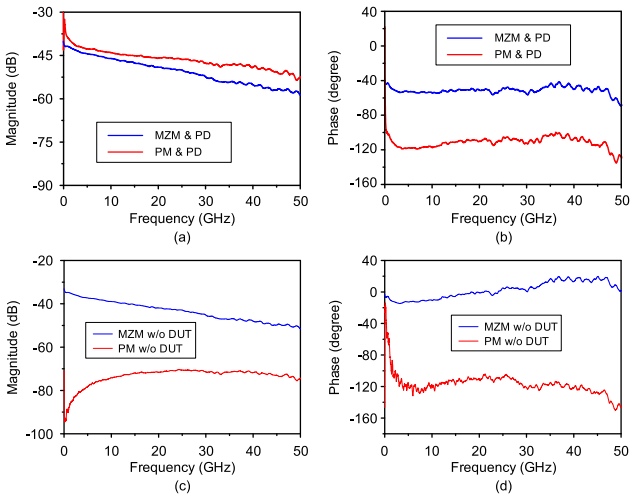

Fig. 2. The (a) magnitude and (b) phase responses of the MZM & PD and the PM & PD, the (c) magnitude and (d) phase responses without a DUT.

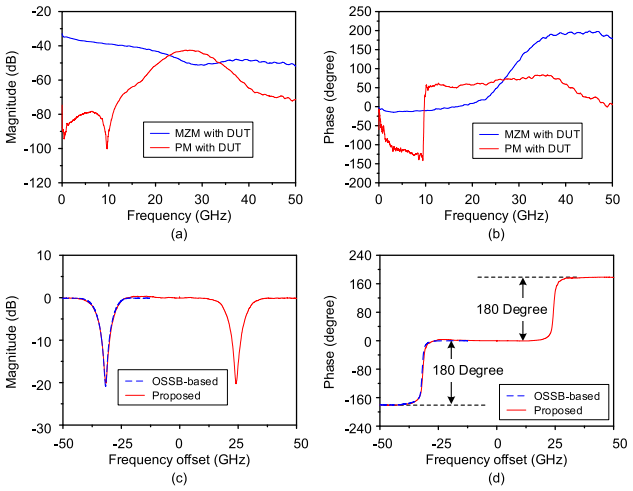

Fig. 3. (a), (b) The magnitude and phase responses measured with the DUT, and (c), (d) the calculated magnitude and phase responses of the DUT.

Figure 3 shows the magnitude and phase responses measured with the DUT, and the calculated responses of the DUT. The DUT is the programmable optical filter which is configured to have two Hilbert-transform-like responses at different frequencies. Since the $H_{MZM}(\omega)$, $H_{PM}(\omega)$, $i_{sys,MZM}(\omega_e)$ and $i_{sys,PM}(\omega_e)$ are already known (as shown in Fig. 2), with the

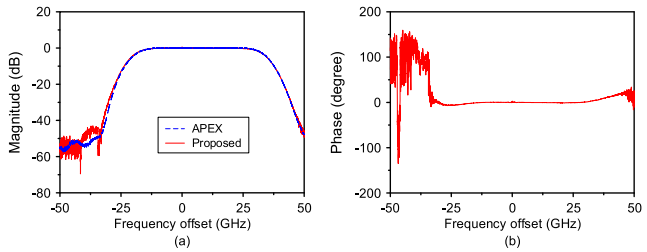

Fig. 4. The measured (a) magnitude and (b) phase responses of the programmable optical filter with the bandpass responses.

transmission responses measured with the DUT, i.e. $i_{\mathrm{MZM}}(\omega_{\mathrm{e}})$ and $i_{\mathrm{PM}}(\omega_{\mathrm{e}})$, as depicted in Fig. 3(a) and (b), the actual magnitude and phase responses of the DUT on both sides of the optical carrier can be calculated based on (15) and (16), with the result shown in Fig. 3(c) and (d). As can be seen, 100-GHz measurement range (from -50 GHz to 50 GHz offset the optical carrier) is obtained by using all 50-GHz devices. As a comparison, the magnitude and phase responses of the DUT on the left side of the carrier are measured by the OSSB-based OVA, which are also plotted in Fig. 3(c) and (d). As can be seen, the responses measured by the two methods are coincident. It should be noted that although the measurement resolution in the experiment is 10 MHz, the resolution can be improved by increasing the measurement points. Theoretically, the proposed ODSB-based OVA can have sub-Hz resolution.

One advantage of the proposed ODSB-based OVA is that the responses of the optical devices with bandpass responses can be measured, which are difficult to achieve by the OSSB-based OVA. Figure 4 shows the measured magnitude and phase responses of the programmable optical filter which is configured to have bandpass responses. The magnitude response measured by a high-resolution optical spectrum analyzer (OSA, APEX AP2040C) with the optical component analysis option is also plotted in Fig. 4 (a). As can be seen, the magnitude response measured by the proposed ODSB-based OVA agrees well with that measured by the commercial instrument. It should be noted that the sweeping sidebands are greatly suppressed when measuring the responses in the stop-band. Therefore, the magnitude and phase responses measured in the stopband contain evident noises.

IV. Conclusion and Discussion

In conclusion, a measurement-range-doubled OVA based on symmetric double-sideband phase modulation and intensity modulation was proposed and experimentally demonstrated. The resolution of the proposed OVA is over 2000 times higher than that of the only commercial OVA (LUNA OVA5000) which is 1.6 pm (corresponding to 200 MHz @ 1550 nm). The magnitude and phase responses of a programmable optical filter which is configured to have two Hilbert-transform-like responses or bandpass responses in a frequency range of 100 GHz were achieved by 50-GHz components. Restricted by the linewidth of the TLS, the frequency resolution is less than 100 kHz. Potentially, sub-Hz resolution is achievable by employing an ultra-narrow-linewidth laser [15]. Benefitting from the large dynamic range of the electrical VNA (typically $\sim$ 130 dB), a dynamic range over 100 dB is available taking into account the degradation from the devices in the system. The measurement accuracies of the magnitude and phase responses are about 0.4 dB and 4 degrees, respectively, according to the performance of the VNA and the stability of the measurement system. The measurement speed is mainly determined by the measurement points and the IF bandwidth of the VNA. In the experiment, the measurement speed is about 2 ms per point with an IF bandwidth of 1 kHz. Hence, it costs around 20 s for one measurement since there are 10000 measurement points. It is worth to mention that the measurement system is wavelength-independent, so that the responses of the optical devices at any wavelengths can be achieved by simply tuning the wavelength of the optical carrier.

References

[1] G. D. VanWiggeren, A. R. Motamedi, and D. M. Barley, "Single-scan interferometric component analyzer," *IEEE Photon. Technol. Lett.*, vol. 15, no. 2, pp. 263–265, Feb. 2003.
[2] D. K. Gifford, B. J. Soller, M. S. Wolfe, and M. E. Froggatt, "Optical vector network analyzer for single-scan measurements of loss, group delay, and polarization mode dispersion," *Appl. Opt.*, vol. 44, no. 34, pp. 7282–7286, 2005.
[3] T. Niemi, M. Uusimaa, and H. Ludvigsen, "Limitations of phase-shift method in measuring dense group delay ripple of fiber Bragg gratings," *IEEE Photon. Technol. Lett.*, vol. 13, no. 12, pp. 1334–1336, Dec. 2001.
[4] J. E. Román, M. Y. Frankel, and R. D. Esman, "Spectral characterization of fiber gratings with high resolution," *Opt. Lett.*, vol. 23, no. 12, pp. 939–941, 1998.
[5] Z. Tang, S. Pan, and J. Yao, "A high resolution optical vector network analyzer based on a wideband and wavelength-tunable optical single-sideband modulator," *Opt. Exp.*, vol. 20, no. 6, pp. 6555–6560, 2012.
[6] S. Pan and M. Xue, "Ultrahigh-resolution optical vector analysis based on optical single-sideband modulation," *J. Lightw. Technol.*, vol. 35, no. 4, pp. 836–845, Feb. 15, 2017.
[7] M. Xue and S. L. Pan, "Influence of unwanted first-order sideband on optical vector analysis based on optical single-sideband modulation," *J. Lightw. Technol.*, vol. 35, no. 13, pp. 2580–2586, Jul. 1, 2017.
[8] M. Xue, S. Pan, and Y. Zhao, "Accuracy improvement of optical vector network analyzer based on single-sideband modulation," *Opt. Lett.*, vol. 39, no. 12, pp. 3595–3598, 2014.
[9] W. Li, J. G. Liu, and N. H. Zhu, "Optical vector network analyzer with improved accuracy based on polarization modulation and polarization pulling," *Opt. Lett.*, vol. 40, no. 8, pp. 1679–1682, 2015.
[10] M. Wang and J. Yao, "Optical vector network analyzer based on unbalanced double-sideband modulation," *IEEE Photon. Technol. Lett.*, vol. 25, no. 8, pp. 753–756, Apr. 15, 2013.
[11] W. Li, W. H. Sun, W. T. Wang, L. X. Wang, J. G. Liu, and N. H. Zhu, "Reduction of measurement error of optical vector network analyzer based on DPMZM," *IEEE Photon. Technol. Lett.*, vol. 26, no. 9, pp. 866–869, May 1, 2014.
[12] T. Qing, M. Xue, M. Huang, and S. Pan, "Measurement of optical magnitude response based on double-sideband modulation," *Opt. Lett.*, vol. 39, no. 21, pp. 6174–6176, 2014.
[13] T. Qing, S. Li, M. Xue, W. Li, N. Zhu, and S. Pan, "Optical vector analysis based on asymmetrical optical double-sideband modulation using a dual-drive dual-parallel Mach–Zehnder modulator," *Opt. Exp.*, vol. 25, no. 5, pp. 4665–4671, 2017.
[14] T. Qing, S. P. Li, M. Xue, and S. Pan, "Optical vector analysis based on double-sideband modulation and stimulated Brillouin scattering," *Opt. Lett.*, vol. 41, no. 15, pp. 3671–3674, 2016.
[15] T. Kessler *et al.*, "A sub-40-mHz-linewidth laser based on a silicon single-crystal optical cavity," *Nature Photon.*, vol. 6, no. 10, pp. 687–692, 2012.